THE MAGNETIC SHEAR–CURRENT AND RÄDLER EFFECTS IN ASTROPHYSICAL TURBULENCE

(JULY 15, 2019, Revision: 1.55)
Draft version July 15, 2019

ABSTRACT

The possibility of explaining shear flow dynamos in terms of a magnetic shear–current effect is examined. Our primary diagnostics is the determination of the turbulent magnetic diffusivity tensor. Using stochastic monochromatic forcing, we show that in the case of magnetically forced turbulence, the quasi-kinematic test-field method yields results similar to a nonlinear method—at least for a simplified set of magnetohydrodynamic equations. For a shear flow in the y direction with negative x derivative, negative values of the component η_{yx} could be suggestive of a shear–current effect and are found in some cases without rotation, but the temporal fluctuations are generally large. In the presence of rotation in the positive z direction, η_{yx} is always negative, which is due to the Rädler effect. Both with and without rotation, small-scale magnetic fields tend to quench the turbulent transport coefficients. We argue that the dynamos found in turbulent shear flow simulations are mainly the result of an incoherent α–shear dynamo.

Subject headings: Sun: magnetic fields — dynamo — magnetohydrodynamics — turbulence

1. INTRODUCTION

Astrophysical bodies such as the Sun and our Galaxy harbour equipartition-strength magnetic fields whose energy density is comparable to the kinetic energy density. Those magnetic fields are produced by fluid motions through dynamo action (Parker 1979). Shear is likely to play a major role in amplifying the magnetic field. While shear is present in the Sun and in the Galaxy, it is particularly important in accretion disks. Indeed, numerical simulations have shown that accretion disks can produce turbulence from a magnetic field by the magneto-rotational instability (MRI; see Balbus & Hawley 1991, 1998), and those magnetic fields are then constantly being replenished by a dynamo instability (Moffatt 1978). This has been seen not only in density-stratified systems (Brandenburg et al. 1995; Stone et al. 1996), where the dynamo can be explained by a turbulent α effect (Krause & Rädler 1980), but also in systems without density stratification (Hawley et al. 1996), where no coherent α effect can be produced. This led to the idea that an incoherent α–shear dynamo could explain the large-scale magnetic fields found in shear flows. By measuring the rms value of α in such a shear flow with the test-field method (TFM), Brandenburg et al. (2008a) concluded that this could indeed the right explanation.

The TFM (Schrinner et al. 2005, 2007) has been used extensively over the past decade to compute turbulent transport coefficients such as the α effect and the turbulent magnetic diffusivity tensor (Brandenburg et al. 2008c). When one employs horizontal averages, both tensors have only four components each. Several important results have been obtained using the TFM; see Brandenburg et al. (2010) for a review. For the purpose of the present work, we note that for turbulent flows without stratification in density and turbulent intensity and with no helicity, all components of the α tensor turn out to vanish within error bars, as expected. The diagonal components of the turbulent magnetic diffusivity tensor, η_{ij} with $i, j = x, y$ are usually always finite and positive. Its off-diagonal components are in general also finite if there is rotation or shear. In conjunction with shear, dynamo action from both effects is possible. The former is generally referred to as $\boldsymbol{\Omega} \times \overline{\boldsymbol{J}}$ or Rädler effect (Rädler 1969a,b). The latter effect is referred to as the shear–current (SC) effect (Rogachevskii & Kleeorin 2003, 2004) and can, for a suitable sign of the relevant off-diagonal component of η_{ij}, lead to dynamo action even without rotation. Both the Rädler and SC effects have been discussed as additional or even major dynamo effects in stars (Pipin & Seehafer 2009), accretion disks (Lesur & Ogilvie 2008; Blackman 2010), and galactic magnetism (Chamandy & Singh 2018).

In the kinematic and quasi-kinematic situations, that is, if the background turbulence is formed solely by velocity fluctuations, the turbulent transport coefficients can be computed from the full knowledge of the velocity field alone. However, when one talks about the *magnetic* Rädler or SC effects, that is, effects which are due to a magnetic background turbulence (Squire & Bhattacharjee 2015a) this may not be the case anymore. A clear example when this distinction makes a decisive difference is the magnetically forced Roberts flow (Rheinhardt & Brandenburg 2010, hereafter RB10). Unlike the kinetically forced Roberts flow (Feudel et al. 2003), where a suitable volume forcing is applied in the momentum equation, and analogous forcing is applied underneath the curl on the right-hand side of the induction equation. For the Roberts flow, there is an α effect that can be computed using the TFM. In the special case when the magnetic field has no variation in the z direction, the horizontally averaged mean magnetic field is just a constant and there is no mean current density. This allows for an independent verification of the values of the α components by computing the electromotive force resulting from an imposed magnetic field (imposed field method). The result from a nonlinear TFM (NLTFM), designed to deal with a magnetic background turbulence, and the imposed field method were found to agree, but were different from those of the quasi-kinematic TFM (QKTFM; see RB10). The QKTFM produced even the wrong sign of α. Thus, the distinction between kinetically and magnetically driven flows can be essential.

It is an open question whether a magnetically forced system corresponds to any physical system. It is possible that it could model the case of a system in which a small-scale dynamo operates, but there is no clear indication in support of such an assertion. Likewise, it is unclear when exactly the QKTFM breaks down. For example, in the case of helically forced high Reynolds number turbulence, Brandenburg et al. (2008a)

found turbulent transport coefficients with the QKTFM that were consistent with what is expected from quenched α_{ij} and η_{ij} tensor components. In their experiments, the magnetic Reynolds number was up to 20 times larger than the critical value for small-scale dynamo action in a nonhelical flow (Haugen et al. 2004), and yet, no evidence for a breakdown of the QKTFM was found.

Coming back to the SC effect, numerical simulations using the QKTFM with a shear flow $\partial \overline{U}_y/\partial x = S < 0$ have resulted in a positive value of η_{yx}, which cannot yield dynamo action (Brandenburg 2005a). The TFM results were consistent with those of analytic approaches (Rädler & Stepanov 2006; Rüdiger & Kitchatinov 2006; Sridhar & Singh 2010; Singh & Sridhar 2011). Simulations have shown, however, that large-scale magnetic fields can be generated in nonhelical shear flows (Brandenburg 2005b; Yousef et al. 2008a,b; Brandenburg et al. 2008a). This was associated either with an incoherent α–shear dynamo (Vishniac & Brandenburg 1997) or with some other type of shear dynamo (Yousef et al. 2008a; Heinemann et al. 2011). There is some evidence, however, that these are actually the same mechanism (Mitra & Brandenburg 2012; Sridhar & Singh 2014; Jingade, Singh & Sridhar 2018).

The idea of an SC effect has been reinvigorated by Squire & Bhattacharjee (2015a,b, 2016), who presented evidence for a *magnetic* SC effect. They first studied the case of a magnetically forced shear flow and later also the kinetically forced case, where small-scale dynamo action was present. The main evidence was obtained by measuring negative η_{yx} both in magnetically forced and small-scale dynamo-active flows. At that time, only the QKTFM was applied, hence the verification of this result with the NLTFM is now in order.

In the presence of rotation, as already mentioned above, there is another important turbulence effect known as the Rädler effect (Rädler 1969a,b). In order for it to lead to dynamo action, shear is needed to stretch the magnetic field, but this is not a turbulence effect and hence distinct from the SC effect. Yousef et al. (2008b) showed that the presence of rotation is not very important and that the dynamo appears similar both with and without rotation. However, this does not constitute evidence for the existence or even dominance of the SC effect, because other mechanisms such as the incoherent α–shear dynamo could operate equally well both with and without rotation. Since rotation has been invoked in several recent papers (Squire & Bhattacharjee 2015a,b, 2016), it will be important to consider both cases separately when determining η_{yx}.

The purpose of the present work is to compute the α_{ij} and η_{ij} tensors for shear flows with and without rotation using the NLTFM and compare with the QKTFM. The NLTFM has been developed so far only for the analysis of a simplified system of magnetohydrodynamic (MHD) equations without the self-advection term, i.e., without the $\boldsymbol{u} \cdot \boldsymbol{\nabla} \boldsymbol{u}$ nonlinearity for the velocity $\boldsymbol{u}$ and without the pressure gradient term. We call this simplified MHD (SMHD), which we compare against full MHD under comparable conditions to assure ourselves that this simplification is not critical to our results.

In some cases, we also inspect the actual dynamo process occurring in our models. We verify that it is broadly consistent with earlier models of turbulent shear flow dynamos studied in the literature. As well as shown in some of the earlier papers, the fluctuations in the instantaneous and local value of α_{ij} are sufficient to explain the dynamo action occur-

ring in the those models. By comparison, the η_{yx} was already found to be of the wrong sign for providing a possible explanation for the observed dynamo process. To study whether the importance of small-scale dynamo action or even of magnetic forcing changes this picture, we study a range of models and measure η_{yx} using different approaches. This helps building some confidence in the validity of those approaches and allows us to determine η_{yx} with sufficient accuracy as the importance of the small-scale fields changes. We begin by exposing those approaches and the different analysis tools in Sect. 2. Next we present results for the various combinations of approaches and tools in turn in Sect. 3. We conclude in Sect. 4.

2. THE BASIC MODEL

In this section we present the basic equations for SMHD and MHD and describe the NLTFM and QKTFM.

2.1. *SMHD*

As stated in the introduction, the equations of SMHD are similar to those of MHD, but without self-advection of the flow and without the pressure gradient. The momentum equation is then analogous to the uncurled induction equation for the magnetic vector potential and we have

$$\mathcal{D}_{xy}\boldsymbol{A} = \boldsymbol{U} \times \boldsymbol{B} + \boldsymbol{F}_{\mathrm{K}} + \eta\nabla^2\boldsymbol{A}, \tag{1}$$

$$\mathcal{D}_{yx}^{2\Omega}\boldsymbol{U} = \boldsymbol{J} \times \boldsymbol{B} + \boldsymbol{F}_{\mathrm{M}} + \nu\nabla^2\boldsymbol{U}, \tag{2}$$

where $\mathcal{D}_{ij}^a = \partial/\partial t + S(\hat{\boldsymbol{x}}_i\hat{\boldsymbol{x}}_j + x\partial/\partial y) - a\epsilon_{ijz}$ is the shear operator (which also includes rotation if $a \neq 0$), so

$$\mathcal{D}_{xy}\boldsymbol{A} = \partial\boldsymbol{A}/\partial t + S(\hat{\boldsymbol{x}}A_y + x\partial\boldsymbol{A}/\partial y), \tag{3}$$

$$\mathcal{D}_{yx}^{2\Omega}\boldsymbol{U} = \partial\boldsymbol{u}/\partial t + S(\hat{\boldsymbol{y}}U_x + x\partial\boldsymbol{U}/\partial y) + 2\boldsymbol{\Omega} \times \boldsymbol{U}, \tag{4}$$

$\boldsymbol{B} = \boldsymbol{\nabla} \times \boldsymbol{A}$ is the magnetic field, $\boldsymbol{J} = \boldsymbol{\nabla} \times \boldsymbol{B}$ is the current density in units where the vacuum permeability is unity, $\boldsymbol{F}_{\mathrm{K}}$ and $\boldsymbol{F}_{\mathrm{M}}$ are kinetic and magnetic forcing functions, respectively, $\boldsymbol{U}$ is the velocity, η is the magnetic diffusivity, and ν is the kinematic viscosity. The main advantage of using SMHD is its simplicity, which allows for the development of an analogous TFM for both equations, as will be reviewed next. The full details are described in RB10.

2.2. *NLTFM*

The evolution equations for the fluctuations in the magnetic vector potential $\boldsymbol{a} = \boldsymbol{A} - \overline{\boldsymbol{A}}$ and the velocity $\boldsymbol{u} = \boldsymbol{U} - \overline{\boldsymbol{U}}$ are given by

$$\mathcal{D}_{xy}\boldsymbol{a} = \overline{\boldsymbol{U}} \times \boldsymbol{b} + \boldsymbol{u} \times \overline{\boldsymbol{B}} + (\boldsymbol{u} \times \boldsymbol{b})' + \boldsymbol{f}_{\mathrm{K}} + \eta\nabla^2\boldsymbol{a}, \tag{5}$$

$$\mathcal{D}_{yx}^{2\Omega}\boldsymbol{u} = \overline{\boldsymbol{J}} \times \boldsymbol{b} + \boldsymbol{j} \times \overline{\boldsymbol{B}} + (\boldsymbol{j} \times \boldsymbol{b})' + \boldsymbol{f}_{\mathrm{M}} + \nu\nabla^2\boldsymbol{u}, \tag{6}$$

where fluctuations are either denoted by lowercase symbols, $\boldsymbol{b} = \boldsymbol{B} - \overline{\boldsymbol{B}}$ for the magnetic field, $\boldsymbol{j} = \boldsymbol{J} - \overline{\boldsymbol{J}}$ for the current density, $\boldsymbol{f}_{\mathrm{K/M}} = \boldsymbol{F}_{\mathrm{K/M}} - \overline{\boldsymbol{F}}_{\mathrm{K/M}}$ for the forcing functions, or by primes. Specifically, we have $(\boldsymbol{u} \times \boldsymbol{b})' = \boldsymbol{u} \times \boldsymbol{b} - \overline{\boldsymbol{u} \times \boldsymbol{b}}$, and likewise for $(\boldsymbol{j} \times \boldsymbol{b})' = \boldsymbol{j} \times \boldsymbol{b} - \overline{\boldsymbol{j} \times \boldsymbol{b}}$. We solve these equations not for the actual mean field resulting from the solutions of Equations (1) and (2), but rather for a set of test fields, $\boldsymbol{B}^{\mathrm{T}}$, namely

$$\boldsymbol{B}^1 = (\cos kz, 0, 0), \quad \boldsymbol{B}^2 = (\sin kz, 0, 0), \tag{7}$$

$$\boldsymbol{B}^3 = (0, \cos kz, 0), \quad \boldsymbol{B}^4 = (0, \sin kz, 0), \tag{8}$$

where $k = 2\pi/L_z$ is the wavenumber of the test field. From the solutions of Equations (5) and (6) we can construct the mean electromotive force, $\overline{\boldsymbol{\mathcal{E}}} = \overline{\boldsymbol{u} \times \boldsymbol{b}}$ and the mean ponderomotive force, $\overline{\boldsymbol{\mathcal{F}}} = \overline{\boldsymbol{j} \times \boldsymbol{b}}$, which are then expressed in terms of the mean field by the ansatzes

$$\overline{\mathcal{E}}_i = \alpha_{ij}\overline{B}_j - \eta_{ij}\overline{J}_j, \tag{9}$$

$$\overline{\mathcal{F}}_i = \phi_{ij}\overline{B}_j - \psi_{ij}\overline{J}_j. \tag{10}$$

Each of the four tensors, α_{ij}, η_{ij}, ϕ_{ij}, ψ_{ij}, has four components, i.e., altogether we have 16 unknowns.

The QKTFM, considered as a functional of $\boldsymbol{u}$, $\overline{\boldsymbol{E}}$, and $\overline{\boldsymbol{B}}$, is linear in $\overline{\boldsymbol{B}}$. A difficulty encountered in the more general case lies in the fact that this is now a priori no longer the case. To deal with this difficulty, RB10 introduced auxiliary fields, $\boldsymbol{u}_0$ and $\boldsymbol{b}_0$, which obey evolution equations similar to Equations (5) and (6), but for zero mean field. In this way, one can split $\overline{\boldsymbol{\mathcal{E}}}$ into a contribution $\overline{\boldsymbol{u}_0 \times \boldsymbol{b}_0}$ that is independent of the mean field and a contribution

$$\overline{\boldsymbol{\mathcal{E}}}_{\bar{B}} = \overline{\boldsymbol{u}_0 \times \boldsymbol{b}_{\bar{B}}} + \overline{\boldsymbol{u}_{\bar{B}} \times \boldsymbol{b}_0} + \overline{\boldsymbol{u}_{\bar{B}} \times \boldsymbol{b}_{\bar{B}}}, \tag{11}$$

which, using $\boldsymbol{u} = \boldsymbol{u}_0 + \boldsymbol{u}_{\bar{B}}$ and $\boldsymbol{b} = \boldsymbol{b}_0 + \boldsymbol{b}_{\bar{B}}$, can be written in two equivalent ways as

$$\overline{\boldsymbol{\mathcal{E}}}_{\bar{B}} = \overline{\boldsymbol{u} \times \boldsymbol{b}_{\bar{B}}} + \overline{\boldsymbol{u}_{\bar{B}} \times \boldsymbol{b}_0} = \overline{\boldsymbol{u}_0 \times \boldsymbol{b}_{\bar{B}}} + \overline{\boldsymbol{u}_{\bar{B}} \times \boldsymbol{b}}. \tag{12}$$

Both are linear functionals of quantities with subscript $\overline{\boldsymbol{B}}$. Likewise, one writes the ponderomotive force as

$$\overline{\boldsymbol{\mathcal{F}}}_{\bar{B}} = \overline{\boldsymbol{j} \times \boldsymbol{b}_{\bar{B}}} + \overline{\boldsymbol{j}_{\bar{B}} \times \boldsymbol{b}_0} = \overline{\boldsymbol{j}_0 \times \boldsymbol{b}_{\bar{B}}} + \overline{\boldsymbol{j}_{\bar{B}} \times \boldsymbol{b}}; \tag{13}$$

see Equations (29) and (30) of RB10. We recall that, although the two formulations in Equations (12) and (13) are mathematically equivalent, they have different stability properties. Here we chose to use in each of them the first one. This implies that $\boldsymbol{j}$ and $\boldsymbol{u}$ are taken from the main run, which is why this is called the ju method; see Table 1 of RB10.

This qualitative description of the NLTFM should suffice to grasp the essentials of this method. Again, for details we refer to RB10.

2.3. QKTFM

We now state here for comparison the governing equations for the QKTFM. They consist of solving just Equation (5), but not Equation (6). The functional is then a linear one, because the velocity from the background simulation is used, so it ignores any influence of the test field. In that case, we only use Equation (9), and Equation (12) reduces simply to

$$\overline{\boldsymbol{\mathcal{E}}}_{\bar{B}} = \overline{\boldsymbol{u} \times \boldsymbol{b}_{\bar{B}}} \quad \text{(QKTFM)}. \tag{14}$$

Again, those details are discussed in full detail in RB10 and were used in Brandenburg et al. (2008b).

2.4. MHD

The full MHD system of equations is more complex because of the occurrence of the pressure gradient, so we have an additional evolution equation for the density, and also the diffusion operator is more complex, namely

$$\mathcal{D}_{xy}\boldsymbol{A} = \boldsymbol{U} \times \boldsymbol{B} + \boldsymbol{F}_{\mathrm{K}} + \eta\nabla^2\boldsymbol{A},$$

$$\rho(\mathcal{D}_{yx}^{2\Omega} + \boldsymbol{U} \cdot \boldsymbol{\nabla})\boldsymbol{U} + \boldsymbol{\nabla}p = \boldsymbol{J} \times \boldsymbol{B} + \rho\boldsymbol{F}_{\mathrm{M}} + \boldsymbol{\nabla} \cdot (2\nu\rho\mathbf{S}),$$

$$(\mathcal{D} + \boldsymbol{U} \cdot \boldsymbol{\nabla})\ln\rho = -\boldsymbol{\nabla} \cdot \boldsymbol{u}. \tag{15}$$

Here, $\mathsf{S}_{ij} = (U_{i,j} + U_{j,i}) - \frac{1}{3}\boldsymbol{\nabla} \cdot \boldsymbol{u}$ are the components of the rate-of-strain tensor $\mathbf{S}$, where commas denote partial differentiation, $\mathcal{D}$ without subscripts is $\partial/\partial t + S\partial/\partial y$, and p is the pressure related to the density via $p = c_{\mathrm{s}}^2\rho$, with $c_{\mathrm{s}} = \text{const}$ being the isothermal sound speed.

2.5. The resetting procedure

The TFM is usually unstable, but this does not usually affect the values of the resulting turbulent transport coefficients, unless one runs over times that are so large that numerical errors become too large. This is why we always reset the small-scale field to zero in regular intervals (usually every 50 turnover times). In the absence of shear, the instability of the TFM turns out to be particularly large. In that case, we ignore all data where the normalized rms value of the TF, $\beta^{\mathrm{T}} = b_{\mathrm{rms}}^{\mathrm{T}}/B_{\mathrm{tot}}$, with $B_{\mathrm{tot}}^2 = \rho U_{\mathrm{rms}}^2 + B_{\mathrm{rms}}^2$ exceeds a certain critical value. We will show below that comparison with a critical value twice as large results in almost the same set of transport coefficients.

2.6. Simulation parameters

The simulations are characterized by magnetic Prandtl and Reynolds numbers as well as the Lundquist number,

$$\mathrm{Pr}_{\mathrm{M}} = \nu/\eta, \quad \mathrm{Re}_{\mathrm{M}} = U_{\mathrm{rms}}/\eta k_{\mathrm{f}}, \quad \mathrm{Lu} = B_{\mathrm{rms}}/\eta k_{\mathrm{f}}. \tag{16}$$

In addition, shear and rotation are characterized by kinetic shear and Coriolis numbers,

$$\mathrm{Sh}_{\mathrm{K}} = S/U_{\mathrm{rms}}k_{\mathrm{f}}, \quad \mathrm{Co}_{\mathrm{K}} = 2\Omega/U_{\mathrm{rms}}k_{\mathrm{f}}. \tag{17}$$

Alternatively, especially for magnetically driven runs, it is advantageous to use the magnetic shear and Coriolis numbers,

$$\mathrm{Sh}_{\mathrm{M}} = S/B_{\mathrm{rms}}k_{\mathrm{f}}, \quad \mathrm{Co}_{\mathrm{M}} = 2\Omega/B_{\mathrm{rms}}k_{\mathrm{f}}. \tag{18}$$

The aspect ratios are $A_{zx} = L_z/L_x$ and $A_{zy} = L_z/L_y$, where L_x, L_y, and L_z are the lengths of the computational domain in all three directions. Unless specified otherwise, we set $A_{zy} = A_{zx}$, i.e., the ratio $A_{yx} = L_y/L_x$ is unity. We define as the basic wavenumber $k_1 = 2\pi/L_x$. Velocities are often normalized by c_{s} and the magnetic field is normalized by the equipartition field strength, $B_{\mathrm{eq}} = \langle\rho\boldsymbol{u}^2\rangle^{1/2}$.

In most of the runs, we find $\eta_{xx} \approx \eta_{yy}$. It is then advantageous to define $\eta_{\mathrm{t}} = (\eta_{xx} + \eta_{yy})/2$ as the isotropic contribution to the turbulent magnetic diffusivity tensor. In some cases we quote the ratio $r_\eta = \eta_{yy}/\eta_{xx}$ of the two diagonal components.

3. RESULTS

We begin by presenting results for magnetically forced SMHD using the NLTFM. This allows for a mathematically consistent system whose mean-field properties can be analyzed rigorously. We then demonstrate the similarity of the results using the QKTFM applied first to SMHD and then to full MHD, before applying it to kinetically forced MHD. We do not specifically discuss here the possibility of generating large-scale magnetic fields and the nature of such a process, which is not a standard dynamo owing to the magnetic forcing.

3.1. NLTFM applied to magnetically forced SMHD

We present first the case of magnetically forced SMHD at small values of Re_{M} and Lu and compare two different forcing wavenumbers, $k_{\mathrm{f}}/k_1 = 5$ and 20, and analyze those systems with the NLTFM. We compare here cases with $\mathrm{Sh}_{\mathrm{M}} =$

TABLE 1
DEPENDENCE ON k_f FOR $Sh_M = -0.20$ AND $Co_M = 0$ IN
MAGNETICALLY FORCED SMHD ANALYZED WITH THE NLTFM.

k_f	Re_M	Lu	η_{xx}/η	η_{yy}/η	η_{xy}/η	η_{yx}/η
5	13	17	4.6 ± 0.2	4.6 ± 0.2	2.2 ± 0.4	-0.1 ± 0.1
20	16	22	6.4 ± 0.1	6.5 ± 0.1	0.6 ± 0.1	-0.0 ± 0.1

TABLE 2
DEPENDENCE ON ASPECT RATIO FOR $Sh_M \approx -0.17$, $Co_M = 0$,
$Re_M \approx 80$ AND $Lu \approx 110$. MAGNETICALLY DRIVEN TURBULENCE
ANALYZED WITH THE NLTFM.

A_{zx}	η_{xx}/η	η_{yy}/η	η_{xy}/η	η_{yx}/η
1	26.9 ± 0.5	27.7 ± 0.7	5.4 ± 0.2	-0.0 ± 0.1
4	27.0 ± 0.8	30.8 ± 0.8	7.9 ± 0.8	0.1 ± 0.1
16	28.6 ± 0.6	31.6 ± 0.8	10.5 ± 0.6	0.1 ± 0.1

TABLE 3
SIMILAR TO TABLE 1, BUT FOR $Co_M \approx 1.5$.

A_{zx}	η_{xx}/η	η_{yy}/η	η_{xy}/η	η_{yx}/η
1	27.2 ± 0.2	31.6 ± 0.4	10.9 ± 0.3	-2.7 ± 0.3
4	28.7 ± 1.0	34.5 ± 1.2	12.6 ± 1.1	-2.1 ± 0.2
16	42.7 ± 1.6	49.2 ± 1.8	65.9 ± 6.0	-2.2 ± 0.2

TABLE 4
DEPENDENCE ON ROTATION RATE FOR $Sh_M = -0.15$ AND 0 USING
$A_{zx} = 4$. MAGNETICALLY DRIVEN SMHD WITH NLTFM.

Co_M	Re_M	Lu	η_{xx}/η	η_{yy}/η	η_{xy}/η	η_{yx}/η
-1.5	82	132	36.5 ± 0.4	35.5 ± 0.5	18.4 ± 0.9	-1.0 ± 0.1
-0.4	82	111	33.1 ± 1.7	36.5 ± 2.8	16.7 ± 3.4	-1.2 ± 0.1
0	115	115	26.0 ± 1.3	28.9 ± 2.0	7.2 ± 1.1	0.0 ± 0.1
0.4	82	111	35.6 ± 0.7	41.0 ± 1.9	34.2 ± 2.8	-2.1 ± 0.1
1.5	82	127	28.7 ± 1.0	34.5 ± 1.2	12.6 ± 1.1	-2.1 ± 0.2
5.7	22	53	12.3 ± 0.7	13.4 ± 0.7	10.7 ± 1.9	-0.4 ± 0.1

TABLE 5
DEPENDENCE ON SHEAR AND ROTATION RATES AT $Re_M \approx 80$ AND
$Lu \approx 120$ FOR MAGNETICALLY DRIVEN TURBULENCE ANALYZED WITH
THE NLTFM. THE ASTERISK DENOTES A RUN WHERE THE ZERO
SOLUTION IS FORCED. IT IS STILL SHORT, SO THE ERRORS ARE LARGE.

$-Sh_M$	Co_M	β^T	η_{xx}/η	η_{yy}/η	η_{xy}/η	η_{yx}/η
0.15	1.5	2404	28.8 ± 1.0	34.6 ± 1.2	12.7 ± 1.1	-2.1 ± 0.2
0.15	1.5	< 200	28.7 ± 1.0	34.5 ± 1.2	12.6 ± 1.1	-2.1 ± 0.2
0	1.6	< 200	25.8 ± 0.4	26.0 ± 0.5	2.0 ± 0.5	-1.4 ± 0.3
0	1.6	< 800	22.1 ± 0.2	22.3 ± 0.1	-1.6 ± 0.0	1.3 ± 0.0
0*	1.6	< 800	36.0 ± 1.4	38.0 ± 1.0	0.1 ± 1.3	1.1 ± 0.8
0	-1.6	< 800	36.5 ± 0.6	35.5 ± 1.1	18.5 ± 0.9	-1.0 ± 0.1

-0.20 (corresponding to $Sh_K = -0.26$), but no rotation. It turns out that the resulting value of η_{yx} is compatible with zero in both cases; see Table 1. The resolution is in both cases 288^3 mesh points. We recall that the values of Re_M and Lu are defined in terms of k_f. Thus, for $k_f/k_1 = 20$, the grid Reynolds number, $u_{rms}\delta x/\nu$ is four times larger, which is in the present example about 14, which does already exceed the typical value that can be simulated at that resolution. We see however, that the components of η_{ij} are similar.

Next, we compare three different aspect ratios $A_{zx} = A_{zy}$ by making the computational domain taller, allowing us to compute η_{ij} for vertical wavenumbers k less than k_1. The result is shown in Table 2 for $A_{zx} = 1$, 4, and 16 using $Re_M \approx 80$ and $Lu \approx 110$. Here the resolution is $144^2 \times 576$ meshpoints. Again, it turns out that η_{yx} is compatible with zero, except possibly for the run with aspect ratio 16, where η_{yx}/η is -0.3 ± 0.2, but here the numerical error may be unrealistically small. Furthermore, in no case does η_{xy} ever vanish. This is interesting in view of the fact that the correlation method (see Brandenburg & Sokoloff 2002) tends to yield negative η_{yx} only if one imposes $\eta_{xy} = 0$ as an additional constraint (Squire & Bhattacharjee 2015a; Shi et al. 2016).

Next, we consider the case with rotation using $Co_M \approx 1.5$. The result is shown in Table 3, again for aspect ratios of one, four, and 16. In these runs we have $Re_M \approx 80$ and $Lu \approx 130$. The sign of η_{yx} is now indeed negative, as would be required for dynamo action by the SC effect. Interestingly, the value of η_{yx} is approximately independent of the aspect ratio and of the wavenumber of the magnetic field. Thus, the idea that large aspect ratios may be important, as suggested by the MRI simulations of Shi et al. (2016), may not be borne out by the present simulations where turbulence is magnetically driven.

In Table 4 we show the dependence of the components of $-\eta_{ij}$ on Co_M. The results show that η_{yx} increases with Co_M, until it reaches a maximum of $-\eta_{yx}$ at $Co_M \approx 1$ and then decreases again. What is curious, however, is that η_{yx} is approx-

imately independent of Co_M. By contrast, in the absence of shear, we expect $\eta_{xy} = -\eta_{yx}$ to change sign when $\mathbf{\Omega}$ changes direction. In the absence of shear, this is still true, as will be confirmed in a moment.

The results presented above suggest that the negative η_{yx} is mainly a consequence of rotation and not of shear. In order to test this, we now also compare with the case without shear. The result is shown in Table 5, where we compare cases with finite rotation ($Co_M \approx 1.6$, corresponding here to $Co_K \approx 2.5$), and either finite shear ($Sh_M = -0.15$, corresponding to $Sh_K = -0.24$) or zero shear. The run with $Sh_M = -0.15$ and $Co_M \approx 1.5$ is the same as that in Table 4 for $Co_M \approx 1.5$. It turns out that without shear, $|\eta_{yx}|$ decreases to about half the value it has with shear. Thus, shear does clearly contributes to enhancing $|\eta_{yx}|$, but it requires the presence of rotation. Furthermore, we always have $\eta_{xy} = -\eta_{yx}$ in the absence of shear. This corresponds to the Rädler effect where

$$\overline{\mathcal{E}} = ... + \delta \mathbf{\Omega} \times \overline{\mathbf{J}}, \tag{19}$$

with $\delta = (\eta_{xy} - \eta_{yx})/2$ being positive (negative) for positive (negative) values of Co_M or Co_K. This is the same sign as for in kinetically driven turbulence; see Brandenburg et al. (2008a).

As explained in Sect. 2.5, the evolution equations advanced by TFM are usually unstable and grow exponentially for sufficiently large values of Re_M, so we need to reset the response to the test field to zero in regular intervals. In our runs without shear, the instability of the TFM is particularly large. In that case, we ignored all data where β^T exceeds a critical value of 400. Comparison with a critical value twice as large resulted in almost the same set of transport coefficients; see rows 3 and 4 in Table 5.

3.2. Comparison with full MHD and kinetically forced cases

The results presented above have all been obtained using SMHD, because this allowed us to apply the NLTFM. Before comparing with full MHD, we first use the QKTFM on magnetically forced SMHD to see whether this method pro-

TABLE 6
COMPARISON BETWEEN STEPS 0–3; SEE TEXT. ALL RUNS HAVE
$\mathrm{Co_K} \approx 1.5$.

Step	$\mathrm{Re_M}$	Lu	η_{xx}/η	η_{yy}/η	η_{xy}/η	η_{yx}/η
0	81	126	28.3 ± 0.6	34.0 ± 0.7	12.2 ± 0.6	-2.2 ± 0.1
1	81	127	30.8 ± 1.1	36.7 ± 1.3	18.6 ± 1.9	-2.2 ± 0.0
2	82	143	18.3 ± 1.0	22.7 ± 1.0	7.2 ± 0.4	-3.0 ± 0.3
3	71	36	15.9 ± 0.3	23.0 ± 1.0	12.4 ± 1.0	-1.2 ± 0.2

TABLE 7
SIMILAR TO TABLE 6, BUT FOR $\mathrm{Co_K} = 0$.

Step	$\mathrm{Re_M}$	Lu	η_{xx}/η	η_{yy}/η	η_{xy}/η	η_{yx}/η
0	116	118	26.1 ± 0.5	29.6 ± 0.6	6.2 ± 0.4	0.2 ± 0.1
1	114	114	25.4 ± 0.7	27.8 ± 0.5	6.9 ± 0.6	-0.0 ± 0.1
2	59	58	11.1 ± 0.2	11.1 ± 0.2	1.8 ± 0.1	0.0 ± 0.0
3	97	26	34.2 ± 3.0	32.8 ± 2.8	20.6 ± 2.7	-0.4 ± 0.4

TABLE 8
COMPARISON OF THE FOUR METHODS FOR STEP 0 OF TABLE 7 SIMILAR
TO TABLE 6, BUT FOR $\mathrm{Co_K} = 0$.

Method	η_{xx}/η	η_{yy}/η	η_{xy}/η	η_{yx}/η
ju	47.4 ± 1.9	43.8 ± 1.2	3.5 ± 0.4	2.9 ± 0.4
bu	37.7 ± 1.3	40.2 ± 1.6	2.6 ± 0.2	0.4 ± 0.0
jb	2.8 ± 0.3	2.6 ± 0.3	0.5 ± 0.1	0.0 ± 0.0
bb	2.7 ± 0.3	2.5 ± 0.3	0.5 ± 0.0	0.0 ± 0.0

TABLE 9
KINETICALLY DRIVEN TURBULENCE ANALYZED WITH THE STANDARD
TFM FOR $\mathrm{Sh_K} \approx -0.3$ AND $\mathrm{Co_K} \approx 3$.

$\mathrm{Pr_M}$	$\mathrm{Re_M}$	Lu	η_{t}/η	r_η	η_{xy}/η	η_{yx}/η
1	28	11	7.7 ± 0.1	1.5	5 ± 0.3	-0.8 ± 0.1
1	72	37	20 ± 0.7	1.5	12 ± 1	-1.2 ± 0.2
1	85	0	56 ± 0.9	1.3	45 ± 2	-5.7 ± 0.6
20	186	156	19 ± 0.4	1.2	-10 ± 2	-1.1 ± 0.1

TABLE 10
$\mathrm{Re_M}$-DEPENDENCE FOR KINETICALLY FORCED TURBULENCE.

$\mathrm{Re_M}$	Lu	η_{t}/η	r_η	η_{xy}/η	η_{yx}/η
0.4	0	0.04	1.05	0.01	0.005
1.4	0	0.4	1.02	0.17	0.06
2.1	0	0.8	1.02	0.42 ± 0.02	0.11 ± 0.01
11	0	12	1.12	6 ± 0.6	0.3 ± 0.2
18	0	20	1.11	8 ± 0.5	0.1 ± 0.1
33	8	32	1.11	15 ± 0.3	0.1 ± 0.0
61	20	35	0.99	14 ± 0.5	-0.5 ± 0.0

TABLE 11
$\mathrm{Pr_M}$ EFFECT FOR KINETICALLY FORCED TURBULENCE.

$\mathrm{Pr_M}$	$\mathrm{Re_M}$	Lu	η_{xx}/η	η_{yy}/η	η_{xy}/η	η_{yx}/η
1	61	20	35.4 ± 0.7	35.0 ± 0.6	13.6 ± 0.5	-0.5 ± 0.0
20	85	93	24.5 ± 1.3	24.7 ± 1.4	6.5 ± 1.1	0.4 ± 0.0

duces incorrect results (step 1). We can then apply the QK-TFM to full MHD (step 2). Finally, we apply is to kinetically forced MHD where small-scale magnetic fields are produced by small-scale dynamo action (step 3). The results of these three steps are shown in Table 6 and compare with the original model (step 0).

Remarkably, the results for η_{yx} are almost unchanged (within error bars) as we go from the NLTFM to the QKTFM, although η_{t} is reduced to about one half. Finally, when changing to kinematic forcing, η_{t} remains roughly unchanged, but now η_{yx} changes to about one half of its former value.

Importantly, however, in all four cases, η_{yx} has the same sign. Furthermore, the ratio $\eta_{yx}/\eta_{\mathrm{t}}$ is roughly the same in the case of magnetically forced SMHD analyzed with NLTFM and in kinetically forced MHD analyzed with the QKTFM.

The comparison between the four steps was shown in Table 6 for $\mathrm{Co_K} \approx 1.5$, but similar results are also obtained for $\mathrm{Co_K} = 0$; see Table 7, except that now the values of η_{yx} are generally closer to zero and more strongly fluctuating.

We now stick with kinetically forced models, keep analyzing the flow with the QKTFM, and vary $\mathrm{Re_M}$. Except for one case, we fix $\mathrm{Pr_M} = 1$, but Lu varies because both η and b_{rms} vary. In one case we have $\mathrm{Lu} = 0$, which has been achieved by setting the initial seed magnetic field to zero. The result is shown in Table 9. It turns out that η_{yx} does not change much as we increase $\mathrm{Re_M}$ from 28 to 185, and Lu increases from 11 to 163. Surprisingly, however, the run without small-scale dynamo ($\mathrm{Lu} = 0$) turns out to have an even more negative value of η_{yx}. Also the diagonal components of η_{ij} have increased by more than a factor of two. This could be compatible with the interpretation that the small-scale dynamo results in an overall suppression of turbulent transport rather than the generation of its own dynamo effect.

Here the aspect ratio is four, but the results are similar also for unit aspect ratio; see Table 10, where we present results for $\mathrm{Pr_M} = 1$ in tabular form. For kinetically forced turbulence, the components of η_{ij} were already computed by Brandenburg et al. (2008a) and then by Squire & Bhattacharjee (2015b); see their Figure 5. The results agree qualitatively in sign and slope with those of Brandenburg et al. (2008a) for $\mathrm{Re} = 1.4$ and variable $\mathrm{Pr_M}$, but in the present case, small-scale dynamo action is possible, as is indicated by the finite values of Lu.

We stress that the negative values of η_{yx}/η for $\mathrm{Re_M} = 61$, as given in Table 10, are the result of temporal averaging over more than 10,000 turnover times. The fluctuations are large; see Fig. 1. In comparison with the incoherent α–shear dynamo, this makes the magnetic SC effect an implausible candidate for explaining dynamo action in such systems. The other components of η_{ij} are also strongly fluctuating, but there is always a well-defined and nonvanishing average both for η_{xy}/η and η_{t}/η.

It is interesting to note that a large magnetic Prandtl number is not always beneficial. In Table 11 we show a corresponding example where, at least for $A_{zx} = 1$, no negative value of η_{yx} is found.

It also turns out that the small-scale dynamo effect plays a surprisingly small role in affecting the SC effect. This is shown in Table 12, where we see that there is no difference in η_{yx} between runs with and without small-scale dynamo. This is different from the case when there is also rotation, as we have seen in Table 9 where in the absence of a small-scale dynamo ($\mathrm{Lu} = 0$), we found $\eta_{yx}/\eta = -5.7$, while with small-scale dynamo ($\mathrm{Lu} = 36$), we found $\eta_{yx}/\eta = -1.3$.

Thus, we can conclude that a negative η_{yx} can be obtained using both magnetically and kinetically forced turbulence, using both MHD and SMHD, analyzed either with the NLTFM or
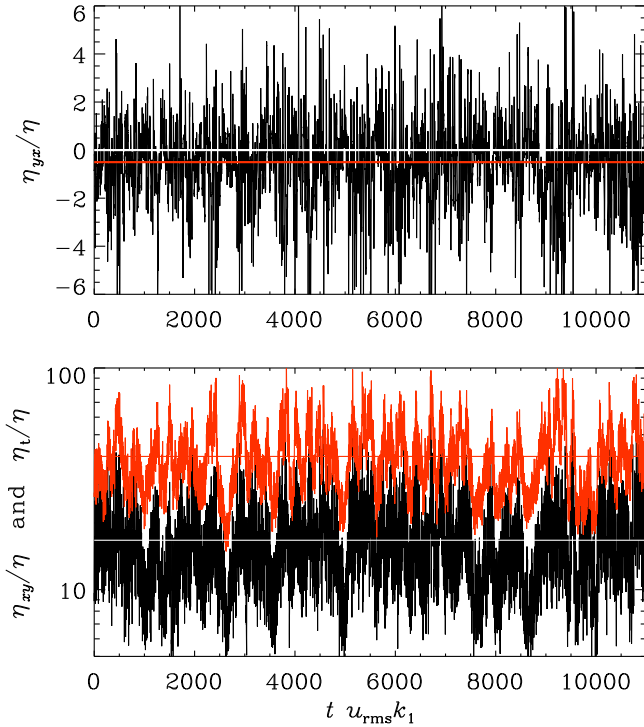
FIG. 1.— Fluctuations of η_{yx}/η (top) and η_{xy}/η, along with η_t/η in red (bottom). In the top panel, the temporal average η_{yx}/η (red) is only slightly below the zero line (white).

TABLE 12
SMALL-SCALE DYNAMO EFFECT FOR KINETICALLY FORCED
TURBULENCE, ANALYZED WITH QKTFM.

Re_M	Lu	η_t/η	r_η	η_{xy}/η	η_{yx}/η
86	94	24.6 ± 1.3	1.01 ± 0.00	6.5 ± 1.1	0.4 ± 0.0
49	0	7.2 ± 0.3	7.4 ± 0.3	4.1 ± 0.5	0.5 ± 0.1

the QKTFM.

In Table 13 we show additional runs without rotation. They show that η_{yx} is either small or positive, being an unfavorable sign for dynamo action. Nevertheless, these runs all exhibit both small-scale and large-scale dynamo action; see Fig. 2. The growth rate of the small-scale dynamo can be determined as $\lambda = \mathrm{d}\ln B_{\mathrm{rms}}/\mathrm{d}t$ during the early phase, and we find $\lambda = 0.045 u_{\mathrm{rms}} k_f$, which is similar to what has been obtained before (Haugen et al. 2004). During a later phase, horizontally averaged mean magnetic and flow fields are being generated.

In Fig. 3 we show the resulting mean magnetic fields. They are superficially similar to those found previously for other forced shear flows; see Yousef et al. (2008a) and Branden-burg et al. (2008a). In this particular run with $Pr_M = 20$, the velocity is obviously much smoother than the magnetic field. This is evident from snapshots of the toroidal velocity and magnetic fields; see Fig. 4. We also clearly see the presence of a mean flow, which is due to what is referred to as a vorticity dynamo; see Elperin et al. (2003); Käpylä et al. (2009). Yousef et al. (2008b) found that its presence does not affect the shear-flow dynamo. To confirm this for the present runs, we show in Fig. 5 the same run as in Fig. 3, but with rotation $q = 1$, corresponding here to $Co_K = 0.9$ (or $Co_M = 0.64$). There is now no mean flow, but the mean magnetic field is qualitatively similar in both cases and compatible with what
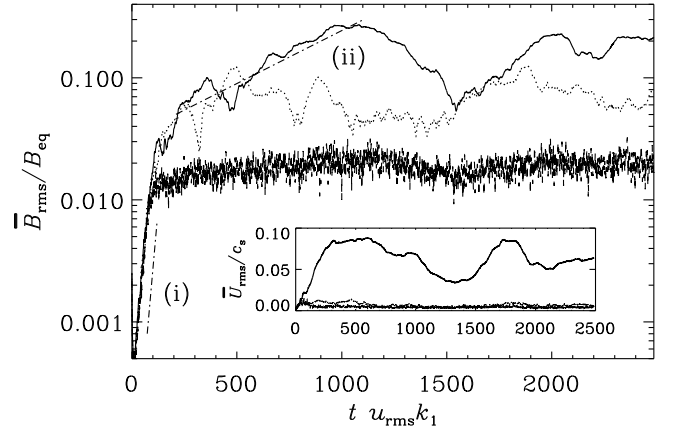

FIG. 2.— Evolution of rms values of xy averaged magnetic field (solid line), yz averaged field (dotted), and xz averaged field (dashed). The dash-dotted slopes denote growth rates (i) $0.045 u_{\mathrm{rms}} k_f$, and (ii) $0.002 u_{\mathrm{rms}} k_f$. The inset shows similarly horizontal averaged rms velocities. $\overline{B}_{\mathrm{rms}}$ and $\overline{U}_{\mathrm{rms}}$ versus t.
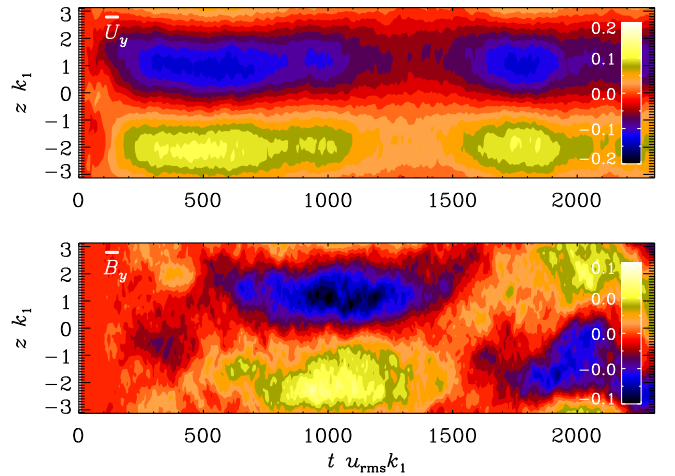

FIG. 3.— Horizontally averaged velocity and magnetic fields as a function of t and z for the run with $Co_K = 0$ of Table 13.
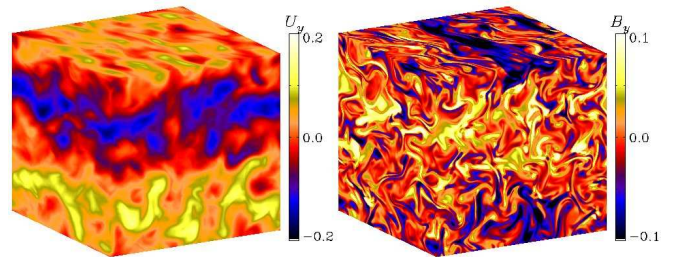

FIG. 4.— Snapshots of U_y and B_y at the last time.

has been found in earlier shear flow dynamos.

With all these preparations in place, we can finally turn to the case without any driving and consider the case when turbulence is driven by just the MRI. Since the MRI is a finite amplitude instability, we used as initial condition a solution where kinetic forcing was turned on. The results are shown in Table 14, again for different values of Re_M, ranging now from 14 to 155 and Lu ranging from 123 to 477. All cases are
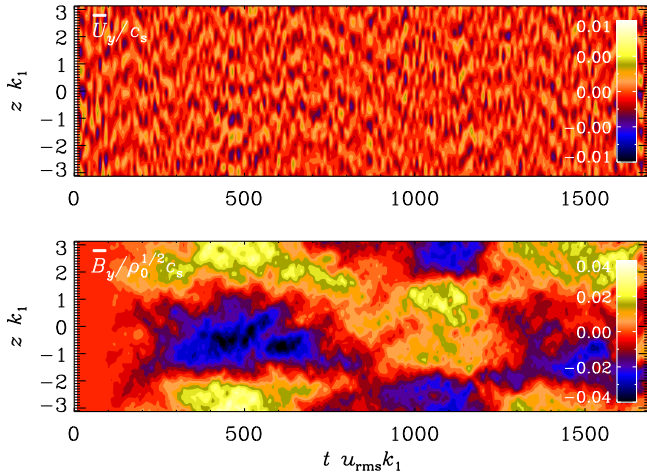
FIG. 5.— Similar to Fig. 3, but for the run with $Co_K = 0.9$ of Table 13.

TABLE 13
KINETICALLY DRIVEN TURBULENCE FOR $Pr_M = 20$, $Lu \approx 230$,
$Sh_M = -0.33$, AND $A_{zx} = 1$ ANALYZED WITH THE STANDARD TFM.

Co_K	$-Sh_K$	Re_M	η_{xx}/η	η_{yy}/η	η_{xy}/η	η_{yx}/η
0	0.25	304	67 ± 3	70 ± 3	17 ± 3	$+1.7 \pm 0.2$
0.9	0.45	170	46 ± 1	50 ± 1	14 ± 1	-1.8 ± 0.3

TABLE 14
RESULTS FOR MRI-DRIVEN TURBULENCE WITH $Pr_M = 20$, $A_{zx} = 4$
AND $A_{zy} = 4$ ($A_{zy} = 1$) DENOTED WITHOUT (WITH) ASTERISK.

Re_M	Lu	η_{xx}/η	η_{yy}/η	η_{xy}/η	η_{yx}/η
*14	123	1.0 ± 0.3	1.0 ± 0.3	1.8 ± 0.3	0.0 ± 0.0
29	161	2.8 ± 1.6	2.6 ± 1.6	4.1 ± 2.1	0.1 ± 0.1
58	204	13.0 ± 0.4	12.7 ± 0.4	19.9 ± 1.8	0.5 ± 0.1
122	440	17.7 ± 2.9	17.3 ± 2.8	17.1 ± 2.4	0.5 ± 0.1
*155	477	42.2 ± 4.1	45.4 ± 4.5	26.8 ± 0.7	0.8 ± 0.1

for $Pr_M = 20$. We see that, toward smaller values of Ω, η_{yx} remains positive. At the same time, the value of η_{xy} remains comparable to those of η_{xx} and η_{yy}. In particular, η_{yx} is positive, so it would not be suitable for explaining the large-scale dynamo action found in this run. The dynamo can therefore neither be explained by the magnetic nor by the ordinary SC effect. This agrees with earlier results by Gressel (2013) and Gressel & Pessah (2015) using the QKTFM, but disagrees with those of Shi et al. (2016) using the correlation method (Brandenburg & Sokoloff 2002).

4. CONCLUSIONS

Our work has illuminated the possible importance of small-scale magnetic fields on the components of the turbulent magnetic diffusivity tensor in mean-field electrodynamics. Those small-scale magnetic fields could be the result of small-scale dynamo action, but in simulations they could also be driven by applying magnetic forcing. In particular, we have inspected the possibility that for shear-flow turbulence, large-scale magnetic fields could be produced by the SC effect, which implies that the poloidal magnetic field is replenished by the off-diagonal component of the turbulent magnetic diffusivity tensor acting on the toroidal magnetic field. This component must have the same sign as the corresponding component of the velocity gradient matrix for this effect to work. We found that this component can, under certain circumstances, have a suitable sign, but it is dominated by strong fluctuations, making it an implausible candidate.

In shear flows with rotation, the relevant off-diagonal component of the magnetic diffusivity tensor is less strongly fluctuating and is found to have the same sign as in the absence of small-scale magnetic fields. In that case, the effect of the small-scale magnetic field is primarily a suppression of the turbulent transparent coefficients, including both the turbulent diffusivity and the Rädler effect, which yields a contribution to the electromotive force proportional to $\mathbf{\Omega} \times \overline{\mathbf{J}}$.

Comparing both quasi-kinematic and fully nonlinear TFMs, we found no indication for a genuinely magnetic effect that can only be described by a fully nonlinear method. In fact, the only case where a genuinely magnetic effect was found is the magnetically forced Roberts flow (RB10). Such a flow lacks Galilean invariance and depends on the position of the forcing function. By contrast, the flows considered here are Galilean invariant owing to the δ-correlated nature of the forcing. While it would be of interest to pursue the possibility of a magnetic SC effect in the presence of flows lacking Galilean invariance, this question is not directly connected with the original goal of explaining the dynamo action found in numerical shear flow experiments that were all caused by Galilean invariant flows. A leading candidate for explaining such magnetic field generation is the incoherent α–shear dynamo (Vishniac & Brandenburg 1997). This mechanism was originally applied to the dynamo action found in unstratified accretion disks (Hawley et al. 1996), which are rotating shear flows. Subsequently, large-scale fields were found also in nonrotating shear flows (Brandenburg 2005b; Yousef et al. 2008a), and the same incoherent α–shear dynamo was found to work also in those.

Of course, real accretion disks are not only rotating, but they are also stratified, so large-scale magnetic fields can then be produced by a coherent α effect, as was already found in Brandenburg et al. (1995). Furthermore, the presence of non-periodic boundary conditions may be important in producing large-scale magnetic fields, especially at low magnetic Prandtl numbers (Käpylä & Korpi 2011), where dynamo action may otherwise not be possible (Lesur & Longaretti 2007).

Finally, we may speculate that earlier suggestions for a magnetic SC effect may have suffered from the assumption that the xy component of the turbulent magnetic diffusivity tensor is zero. While this component is not "needed" for dynamo action, our present work shows that it was small. Relaxing this assumption can imply an unfavorable sign of η_{yx}, as detected by the correlation method (Amelia Hankla, private communication).

REFERENCES

Balbus, S. A., & Hawley, J. F. 1991, ApJ, 376, 214
Balbus, S. A. & Hawley, J. F. 1998, Rev. Mod. Phys., 70, 1
Blackman, E. G. 2010, Astron. Nachr., 331, 101
Brandenburg, A. 2005a, Astron. Nachr., 326, 787
Brandenburg, A. 2005b, ApJ, 625, 539

Brandenburg, A., & Sokoloff, D. 2002, Geophys. Astrophys. Fluid Dyn., 96, 319
Brandenburg, A., Chatterjee, P., Del Sordo, F., Hubbard, A., Käpylä, P. J., & Rheinhardt, M. 2010, Phys. Scr., T142, 014028

8

Brandenburg, A., Nordlund, Å., Stein, R. F., & Torkelsson, U. 1995, ApJ, 446, 741

Brandenburg, A., Rädler, K.-H., Rheinhardt, M., & Käpylä, P. J. 2008a, ApJ, 676, 740

Brandenburg, A., Rädler, K.-H., Rheinhardt, M., & Subramanian, K. 2008b, ApJ, 687, L49

Brandenburg, A., Rädler, K.-H., & Schrinner, M. 2008c, A&A, 482, 739

Chamandy, L., & Singh, N. K. 2018, MNRAS, 481, 1300

Elperin, T., Kleeorin, N. & Rogachevskii, I. 2003, Phys. Rev. E, 68, 016311

Feudel, F., Gellert, M., Rüdiger, S., Witt, A., & Seehafer, N. 2003, Phys. Rev. E, 68, 046302

Gressel, O. 2013, ApJ, 770, 100

Gressel, O., & Pessah, M. E. 2015, ApJ, 810, 59

Haugen, N. E. L., Brandenburg, A., & Dobler, W. 2004, Phys. Rev. E, 70, 016308

Hawley, J. F., Gammie, C. F., & Balbus, S. A. 1996, ApJ, 464, 690

Heinemann, T., McWilliams, J. C., & Schekochihin, A. A. 2011, Phys. Rev. Lett., 107, 255004

Jingade, N., Singh, N. K., & Sridhar, S. 2018, eprint arXiv:1802.04567

Käpylä, P. J., & Korpi, M. J. 2011, MNRAS, 413, 901

Käpylä, P. J., Mitra, D., & Brandenburg, A. 2009, Phys. Rev. E, 79, 016302

Krause, F., & Rädler, K.-H. 1980, Mean-field Magnetohydrodynamics and Dynamo Theory (Oxford: Pergamon Press)

Lesur, G., & Longaretti, P.-Y. 2007, A&A, 378, 1471

Lesur, G., & Ogilvie, G. I. 2008, A&A, 488, 451

Mitra, D., & Brandenburg, A. 2012, MNRAS, 420, 2170

Moffatt, H. K. 1978, Magnetic Field Generation in Electrically Conducting Fluids (Cambridge: Cambridge Univ. Press)

Parker, E. N. 1979, Cosmical magnetic fields (Clarendon Press, Oxford)

Pipin, V. V., & Seehafer, N. 2009, A&A, 493, 819

Rädler, K.-H. 1969a, Monats. Dt. Akad. Wiss., 11, 194

Rädler, K.-H. 1969b, Monats. Dt. Akad. Wiss., 11, 272

Rädler, K.-H., & Stepanov, R. 2006, Phys. Rev. E, 73, 056311

Rheinhardt, M., & Brandenburg, A. 2010, A&A, 520, A28 (RB10)

Rogachevskii, I., & Kleeorin, N. 2003, Phys. Rev. E, 68, 036301

Rogachevskii, I., & Kleeorin, N. 2004, Phys. Rev. E, 70, 046310

Rüdiger, G., & Kitchatinov, L. L. 2006, Astron. Nachr., 327, 298

Schrinner, M., Rädler, K.-H., Schmitt, D., Rheinhardt, M., & Christensen, U. 2005, Astron. Nachr., 326, 245

Schrinner, M., Rädler, K.-H., Schmitt, D., Rheinhardt, M., & Christensen, U. R. 2007, Geophys. Astrophys. Fluid Dyn., 101, 81

Shi, J.-M., Stone, J. M., & Huang, C. X. 2016, MNRAS, 456, 2273

Singh, N. K. & Sridhar, S. 2011, Phys. Rev. E, 83, 056309

Squire, J., & Bhattacharjee, A. 2015, Phys. Rev. E, 92, 053101

Squire, J., & Bhattacharjee, A. 2015, ApJ, 813, 52

Squire, J., & Bhattacharjee, A. 2016, J. Plasma Phys., 82, 535820201

Sridhar, S. & Singh, N. K. 2010, J. Fluid Mech., 664, 265

Sridhar, S. & Singh, N. K. 2014, MNRAS, 445, 3770

Stone, J. M., Hawley, J. F., Gammie, C. F., & Balbus, S. A. 1996, ApJ, 463, 656

Vishniac, E. T., & Brandenburg, A. 1997, ApJ, 475, 263

Yousef, T. A., Heinemann, T., Schekochihin, A. A., Kleeorin, N., Rogachevskii, I., Iskakov, A. B., Cowley, S. C., & McWilliams, J. C. 2008a, Phys. Rev. Lett., 100, 184501

Yousef, T. A., Heinemann, T., Rincon, F., Schekochihin, A. A., Kleeorin, N., Rogachevskii, I., Cowley, S. C., & McWilliams, J. C. 2008b, Astron. Nachr., 329, 737